COBEM 2021 26th International Congress of Mechanical Engineering
ABCM Associação Brasileira de Engenharia e Ciências Mecânicas
November 22-26, 2021, Virtual Congress, Brazil

COB-2021-1541
AIRCRAFT PILOT MODELING DURING NOSE WHEEL STEERING CONTROL

Pablo Milheiro
Luiz Carlos Sandoval Góes
Instituto Tecnológico de Aeronáutica (ITA) - Praça Marechal Eduardo Gomes, 50 - Vila das Acacias, São José dos Campos - SP, Brazil
pablomilheiro@gmail.com
goes@ita.br

Daniel Bueno Silveira Lima
EMBRAER - Av Brigadeiro Faria Lima, 2170 - Putim, São José dos Campos - SP, Brazil
daniel.lima@embraer.com.br

Abstract. *Aircraft on-ground maneuvering is made manually by the pilot, the aircraft and the pilot close a loop forming one system that performs a trajectory, the analysis of the steering control system in closed-loop is crucial to prevent the aircraft from unstable events, which may cause damage to the plane, injured passengers, or even fatalities. This research goal is to propose a human pilot model to provide inputs for the simulation of nose wheel steering systems. The proposed model uses the heading error between the plane and a look-ahead reference as the main visual cue, that is feedback using a linear compensator. State feedback is considered assuming that the pilot can sense the yaw rate, a feedforward control is also included to contemplate the action made only based on the desired trajectory. For simulation purposes, a three degrees-of-freedom aircraft and steering system models are used in Matlab/Simulink. Finally, the grey-box identification is performed using the Parameter Estimator app in Simulink to adjust parameters for two behaviors. The pilot model performance is discussed, the results show the capability of the model to fit two different behaviors, moreover, the main parameters that should differ between behaviors are highlighted.*

Keywords: *Modeling and simulation, aircraft landing gears, human factors, nose wheel steering.*

1. INTRODUCTION

The human operator model has been developed to assess human behavior during manual tasks when controlling machines in different industries, Zaychik *et al.* (2012). In the aviation industry, human pilot models help aircraft manufactures to design aircraft control systems and evaluate aircraft controllability. Taxiing is one of many tasks that are made manually by the pilot, the pilot and the aircraft close a loop forming just one system that receives ground indications and external disturbances as inputs and performs a trajectory on the ground as output. Depending on the steering mechanism it can cause a closed-loop instability that may lead to a runway excursion compromising the safety of the system.

Xu *et al.* (2017) presented a history of main pilot models developed and improved by several authors. As a summary of Rasmussen (1983) results, human behavior is shown to be classified into three major types: skill-based, rule-based, and knowledge-based. The rule-based behavior refers to discrete decision-making, that is used during situations like a loss of a certain aircraft system, in which the pilot needs to perform a previously known correction. Knowledge-based behavior is related to control capability when dealing with unfamiliar environments in which the pilot has unusual and unknown circumstances. Therefore, when a pilot follows a previously known mission statement applying continuous actions to complete the task, he/she performs through skill-based behavior. For skill-based pilot behavior, Xu *et al.* (2017) also classifies well-known models in three major groups: models based on control theory, models based on human physiology, and models based on intelligence techniques. This paper considers skill-based behavior, proposing a model based on control theory.

Models based on control theory consider that the pilot's behavior is similar to a feedback controller, with one or more closed loops. McRuer and Graham (1963) introduced the crossover model for compensatory tracking purposes. This model considers a linear model associated with a remnant, which is a colored noise injection to accounts for nonlinear effects and unintended noise. The main goal of the model is to generalize a human operator as a lead or lag compensator, with time delay, in such a way to perform a stable and appropriate control. Drop (2016) shows an implementation of the crossover model associated with a feedforward control to provide part of the pilot action that is based upon the tracked mission profile. The application of the McRuer crossover model to curve driving tasks was presented by van der El *et al.* (2014), the authors also used feedforward control and considered the driver anticipation by applying a look-ahead time,

two points were used in the model: a near and a far viewpoint. The near viewpoint is the input for the feedforward control, which was found to be less expressive than the compensatory contribution that uses the far viewpoint. Nieuwenhuizen *et al.* (2008) presented a multichannel pilot model, showing that the human operator can also close the control loop with perceived states and not only with the visual error.

Aircraft on-ground dynamics simulations can provide essential insights about the airplane landing gear design before the manufacturing of a prototype or even avoiding the high costs of flight tests. Several pilot models were developed for in-flight control tasks as shown in Lone and Cooke (2014). This paper intends to extend the research about pilot models for taxiing tasks, aiming at its use for the evaluation of steering systems during on-ground maneuvers, the identification of the model parameters is also presented.

Section 2 describes the on-ground dynamics of the aircraft and a mechanical steering system, that connects the pilot rudder pedals to the nose landing gear (NLG). In section 3 the pilot model for steering control is proposed using multiple closed-loops and a feedforward control. The grey-box identification of the model is detailed in section 4. Finally, a comparison between two model parameters identified by different experiments is made, showing the main parameters that differ between behaviors.

2. ON-GROUND DYNAMICS

2.1 Aircraft model

This work is focused on the pilot model for ground control, the development of a sophisticated aircraft ground dynamics model would require more computational capabilities, making it difficult to test new features and modifications in a fast way. Simplified models are usually used during the development of pilot/driver models, after the development and validation of the model a more detailed plant model can be used for evaluation of the vehicle stability, loads, and dynamics.

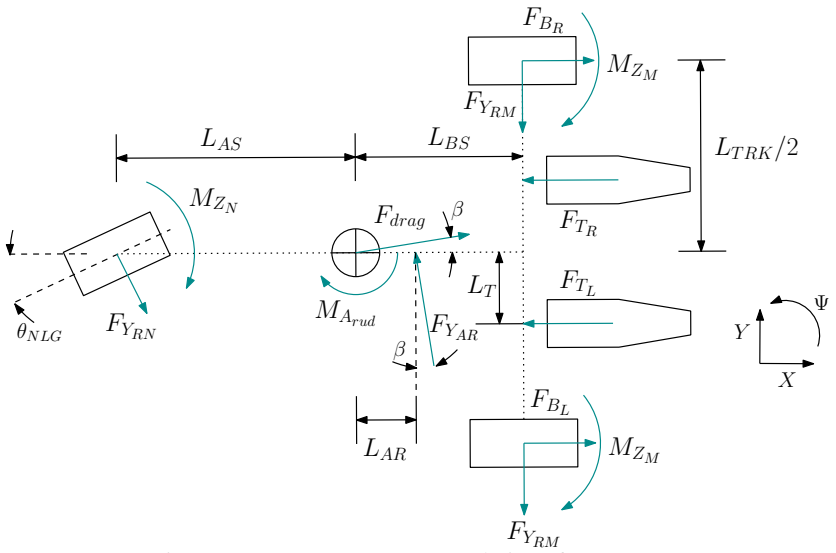

Figure 1: Forces, moments, and aircraft geometry.

Figure 1 shows the forces, moments, and moment arms on the tricycle landing gear basic geometry. The presented model only considers three degrees of freedom: X-axis displacement, Y-axis displacement, and the yaw Ψ. The landing gear shock absorbers and tires deflections dynamics are neglected, this approximation has less impact for low speed and high radius turns, tire lateral forces and moments generated by the main landing gear (MLG) are also considered to be equal for the left and right tires. Therefore, the forces acting and considered are: NLG and MLG tire lateral forces $F_{Y_{RN}}$ and $F_{Y_{RM}}$, and self aligning moments M_{Z_N} and M_{Z_M}, drag force F_{drag}, lateral aerodynamic force $F_{Y_{AR}}$, rudder moment $M_{A_{rud}}$, brakes forces F_{B_L} and F_{B_R}, and engines thrust F_{T_L} and F_{T_R}. Thrust and brakes are used to maintain the aircraft's ground speed constant. Considering the forces and moments, the equations of motion of the three degrees of freedom model are obtained for the ground fixed coordinates system, where $\ddot{X}$, $\ddot{Y}$, and $\ddot{\Psi}$ are the X-axis, Y-axis and yaw accelerations, respectively, R is the yaw rate, L_{AS} is the distance from the center of gravity (CG) to the NLG, L_{BS} is the distance from CG to MLG, L_{AR} is the distance between the aerodynamic center and the CG, L_{TRK} is the track width between MLG tires, L_T is the distance between the engines and the aircraft centerline, and β is the aerodynamic sideslip angle. M_{CG} represents the mass and I_{ZZ} the yaw rotational moment of inertia.

$$\ddot{X} = \frac{1}{M_{CG}}[F_{Y_{RN}}\sin(\theta_{NLG}+\Psi) + 2F_{Y_{RM}}\sin(\Psi) - F_{Y_{AR}}\sin(\beta+\Psi) + F_{drag}\cos(\beta+\Psi) + (F_{B_L}+F_{B_R})\cos\Psi - (F_{T_L}+F_{T_R})\cos\Psi] \tag{1}$$

$$\ddot{Y} = \frac{1}{M_{CG}}[-F_{Y_{RN}}\cos(\theta_{NLG}+\Psi) - 2F_{Y_{RM}}\cos(\Psi) + F_{Y_{AR}}\cos(\beta+\Psi) + F_{drag}\sin(\beta+\Psi) + (F_{B_L}+F_{B_R})\sin\Psi - (F_{T_L}+F_{T_R})\sin\Psi] \tag{2}$$

$$\ddot{\Psi} = \dot{R} = \frac{1}{I_{ZZ}}[-M_{Z_N} + F_{Y_{RN}}\cos(\theta_{NLG})L_{AS} - 2M_{Z_M} - 2F_{Y_{RM}}L_{BS} + F_{Y_{AR}}\cos(\beta)L_{AR} - F_{T_L}L_T + F_{T_R}L_T + F_{B_L}L_{TRK}/2 - F_{B_R}L_{TRK}/2] \tag{3}$$

2.2 Steering dynamics

Even though hydraulic or electric actuation has many advantages for steering systems, for smaller executive jets or piston aircraft, it is possible to design a mechanical steering system that can save space, weight and reduce complexity. Moreover, the ground forces are lower and the pilot is capable to actuate the system through a sequence of mechanical levers and arms. The challenge of the mechanical steering system design is that the system needs to respond in different ways from the pilot input depending on the ground speed, for higher speeds the system has to steer in smaller angles when receives greater pilot inputs so it can maintain stability during a take-off. Additionally, when the aircraft is at lower speeds the system has to steer at greater angles, delivering to the pilot the capability to do small radius turns during taxi. In order to provide the system the above capability, a flexible element can be used between the pilot pedals and the NLG, this element connects two levers as shown in Fig. 2b.

Figure 2 shows the mechanical model and the bond-graph of the same system. Some forces play an important role in the system described and were considered, the forces between the tire and the runway cause a moment due to the rake angle M_{Z_N}, a self-aligning moment $M_{Z_{RA}}$ and also a bearing friction torque at the nose landing gear axis T_{frc}. The pilot pedal is connected to the steering system with a spring that is considered to have a stiffness K_s, and damping of B_s. The pedals are also connected to the rudder surface which generates aerodynamic forces and also adds a rotational inertial, however, the rudder contribution was not considered, assuming that the pilot would be able to generate the required force to command directly the position, for this reason, the bond-graph model considers only a flow injection of the pedal angular velocity ω_{ped}.

The steering dynamic equations were achieved using the bond graph model described in Fig. 2a. The model has two levers disposed in a planar motion with one inertance element I:J_1 associated to one of the 1-junction (NLG angular velocity ω_{NLG}), associated with this velocity there is also a resistor element R with friction coefficient C_{frc_1}. The velocity of pedal lever ω_{ped} is imposed by the pilot during control, being the system input. The moments generated by the ground forces and the bearing friction are connected to the ω_{NLG} 1-junction. Modulated transformers are used to transform the angular velocities to (x_1', y_1') and (x_2', y_2') coordinates, indicated by $V_{x_1'}$ and $V_{y_1'}$ for the NLG lever and $V_{x_2'}$ and $V_{y_2'}$ for the pedal lever, these transformers depends on the levers length L_1 and L_2 and are modulated by the steering angles. Then, the velocities are transformed to the flexible element axis, this time, the modulation is made by the flexible element angle θ_s. Analyzing the bond graph structure it is possible to notice that no differential causality was found leaving the system with two integral causalities, one in the inertance element and another in the compliance element representing the flexible element stiffness. The steering dynamic equations are presented below, in which θ_{NLG}, θ_{ped} and d_s are the NLG angle, the pedal angle, and the flexible element deformation, respectively.

$$\dot{\omega}_{NLG} = \frac{1}{J_1}\Bigg[- M_{ZN} - M_{Z_{RA}} - T_{frc} - C_{frc_1}|\omega_{NLG}|\,\omega_{NLG} + \left(B_s(\omega_{NLG}L_1\cos(\theta_{NLG}+\theta_s) + \omega_{ped}L_2\cos(\theta_{ped}+\theta_s)) + \frac{1}{C}d_s\right)(-L_1\cos(\theta_{NLG}+\theta_s))\Bigg] \tag{4}$$

$$\dot{d}_s = \omega_{NLG}L_1\cos(\theta_{NLG}+\theta_s) + \omega_{ped}L_2\cos(\theta_{ped}+\theta_s) \tag{5}$$

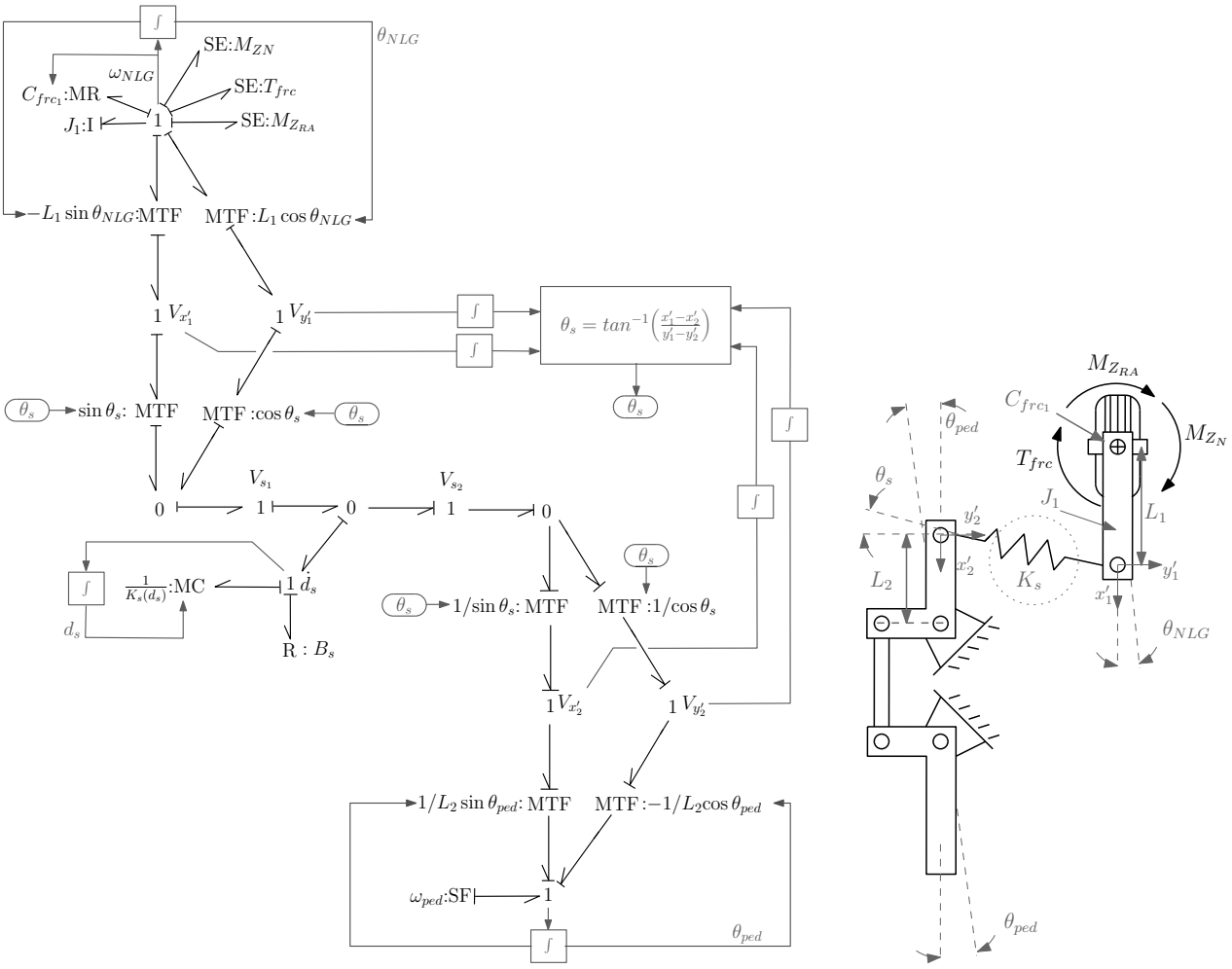

(a) Steering system bond graph

(b) Steering elements and moments

Figure 2: Steering system model using (a) bond graph and (b) physical system representations.

3. PROPOSED PILOT MODEL

When on the ground, the pilot has access to ground references that are used as visual cues to control the aircraft, he/she also has information about some aircraft states, as the human can sense accelerations and angular velocities without visual references. To better model the pilot during steering, it is necessary to realize the main characteristics of a human operator when steering a vehicle, for this reason, models of human drivers found in the literature were also considered in this work. Macadam (2003) characterized the human driver aiming at vehicle steering and braking control. Some characteristics reported are suitable for the human pilot role during steering control, such as time delay and threshold limitations, motion perception, proprioceptive and haptic information, preview capability, adaptation provision, and an internal plant model. The preview capability is an important aspect for the pilot when controlling the aircraft on the ground. This characteristic allows the pilot to perceive the upcoming path, in practice, from the cockpit it is possible to see the ground lines of the airport that serves as a reference. For the proposed model it is assumed that the pilot considers a forward fixed point from a look-ahead distance (LAD). Different approaches can be used to consider the perceived error ahead, a simpler manner is to use only the error between the aircraft heading and the direction of the closest intersection between the LAD radius and the desired curve, this approach is known as follows the carrot by the research area of autonomous ground vehicles, Amer *et al.* (2017). Figure 3 shows the visual cue adopted.

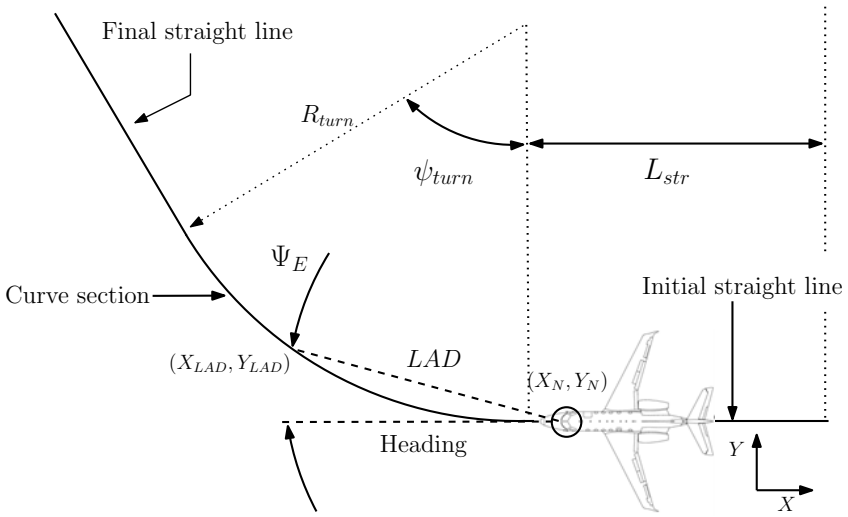

Figure 3: Visual error representation and constant radius turn maneuver.

This paper considers a constant radius curve maneuver for the simulations and experiments, as shown in Fig. 3. The point (X_N, Y_N) represents the position of the NLG that is assumed to be very close to the cockpit, and the coordinates (X_{LAD}, Y_{LAD}) represents the intersection of the LAD range and the desired path, the LAD parameter is calculated by multiplying the ground speed V_{CG} by the anticipation time T_{LAD}. R_{turn} is the turning radius of the maneuver, ψ_{turn} is the total turn angle and L_{str} is the first straight section length.

The crossover model was first introduced to model the human operator during compensatory control, van der El *et al.* (2014) proposed a driver model that is suitable for curve driving, which includes not only the feedback loop but also a feedforward control based on the assumption that the driver can use the information of the tracking path. The possibility of using plant states feedback is also mentioned, as the driver would be able to perceive the vehicle's motion and use this information to improve control. Based on the curve tracking model, the pilot model shown in Fig. 4 is proposed for the steering control task.

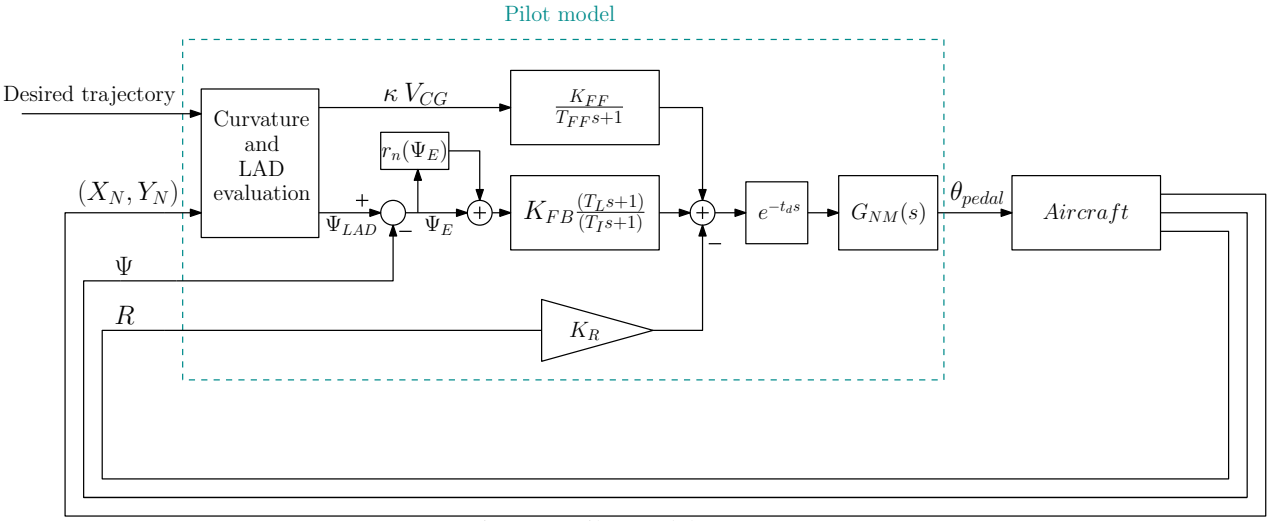

Figure 4: Pilot model structure.

The compensatory feedback contribution receives the visual cue error Ψ_E, which is the angle between the aircraft heading and a preview point by a look-ahead distance. The $T_{LAD_{FB}}$ parameter calibrates the preview point, closer points will increase the lateral error relevance but may cause instabilities, instead, farther preview points may cause the model to cut corners. Based on the crossover model, a lead compensator $G_{FB}(s) = K_{FB}\frac{T_L s+1}{T_I s+1}$ is used for the look-ahead point error, with a feedback gain K_{FB}, a lead time T_L, and a lag time T_I. Regarding the perception of the error by the pilot, it cannot be precisely made during the visual cueing, moreover, the pilot control can also have nonlinear contributions that will not be captured by the linear compensator. To account for that, a remnant function r_n is proposed to be positioned before the compensator. The remnant was initially proposed as a colored noise added up to the crossover model output, recently studies compared the presence of the remnant for different tracking and preview tasks van der El *et al.* (2019), although it is shown by the author that the remnant is independent of the task type and preview time, during tests of

the model proposed by this paper the introduction of the remnant before the linear compensator was more efficient for fitting the data, furthermore, the modulation of the colored noise w_c by the look-ahead heading error Ψ_E, shown below, presented even better results, for the colored noise the $H_n(s)$ filter is used, with a gain K_n and a filter time T_n,

$$r_n(\Psi_E) = w_c\, \Psi_E, \tag{6}$$

$$H_n(s) = \frac{K_n}{(T_n s + 1)^2}. \tag{7}$$

The yaw rate R can be perceived visually when the pilot looks at the airport surroundings and also by the vestibular system inside the inner ear, as a result, the model does not consider a threshold for the angular velocity perception and summarizes it as mainly visual for slow ground maneuvers. The yaw rate loop also helps to improve the pilot-aircraft overall stability, working as a dumper for angular velocity response. The R state feedback control loop is closed with a gain K_R.

The feedforward control accounts for the command that does not depend on the look-ahead error, this component is proper for the path tracking in which the pilot has total access to reference and not only the error, which is found on pure compensatory human control, Drop (2016). When it is assumed a steady-state equilibrium in a curve of constant radius turn, the lateral velocity can be neglected and the yaw rate R is constant, and it would be required to be equal to the curvature κ times the ground speed V_{CG}, Zhou and Peng (2009) shows this relation for the bicycle model. Considering that the curvature of the path and the aircraft speed is directly related to the needs of a command, the pilot is assumed to react proportionally to this product, filtering high-frequency changes. The response to the curvature of the desired trajectory is also considered to be anticipated by a time $T_{LAD_{FF}}$, which is expected to be lower than the feedback anticipation $T_{LAD_{FB}}$, Drop (2016). For the maneuver of constant radius analyzed in this paper the ground speed is constant, however, the curvature is zero during the straight sections and is equal to the inverse of the radius during the turn section. The desired yaw rate ($R_d = \kappa V_{CG}$) can be interpreted as the necessary output, the greater it gets, greater inputs are needed to follow the path. This approach indicates the main reason why the curvature times the speed is important for the feedforward control contribution, for simplicity the model considers a major gain K_{FF} and a filter time T_{FF}, as follows:

$$G_{FF}(s) = K_{FF} \frac{1}{(T_{FF} s + 1)}. \tag{8}$$

The proposed model is composed of three main commands that are derived by the desired trajectory, the pilot position, the aircraft heading, and the yaw rate. These cues are considered to be perceived mainly by the pilot vision, for this reason, a single time delay is applied to all processed information to accounts for brain processing time and visual perception. The motion lag of the human controller is also considered associated with muscular lag dynamics, this accounts for the time needed to move the body and apply the processed position on the rudder pedals or inceptor. McRuer and Graham (1963) introduced the neuromuscular dynamics using a first-order lag that considered the mechanical impedance of the pilot and the manipulator together. More recent works used second-order dynamics to model the neuromuscular system, Zaal *et al.* (2009); Nash and Cole (2018). Hess (2005) used a natural frequency $\omega_n = 10$ rad/s and a damping factor $\xi_n = 0.707$ to map the legs actuating dynamics with a second-order system.

$$G_{NM}(s) = \frac{\omega_n^2}{s^2 + 2\xi_n \omega_n s + \omega_n^2} \tag{9}$$

4. IDENTIFICATION OF PILOT MODEL PARAMETERS

The pilot model parameters depend mainly upon the pilot experience, reaction time response, and skills. The objective of this pilot modeling is to create a set of representations of human pilot behaviors to better test a new aircraft design throughout simulations and before the manufacturing of prototypes and rigs. The parameter identification procedure is important to mimic each individual pilot behavior. A grey-box identification is proposed in this work, where the model structure is considered mapped, Fig. 4, and only the model parameters have to be found using experimental data.

4.1 Pilot-in-the-loop experiment

Pilot-in-the-loop experiments were realized in order to generate data for the identification procedure, the on-ground dynamics model presented before was implemented in Simulink for the simulations, the experiment was designed following the diagram of Fig. 5. Several rounds were made by the same operator controlling the aircraft in the real-time simulation, two experiments data were saved for the identification, the first when the operator was in one of the first tries and the second one the last round, that the operator was able to have a better performance.

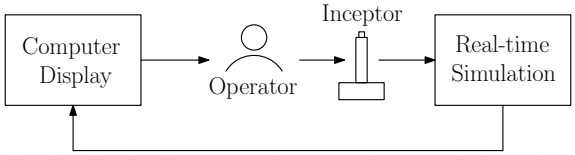

Figure 5: Pilot-in-the-loop experiment using a real-time simulation.

The Simscape Multibody environment was used to perform the visualization of the simulation, displaying the perspective view inside of the aircraft as shown in Fig. 6b, the constant radius maneuver shown in the Fig. 3 was detailed visually using the 3D tool with a yellow center line representing the taxiway markings on the airport ground, Fig. 6a, the maneuver was defined with $L_{str} = 60$ m, $R_{turn} = 60$ m, $\psi_{turn} = 1.2217$ rad, and a constant speed $V_{CG} = 7.717$ m/s. The deflection of the inceptor data is considered as the output of the operator and considered to be the steering command position θ_{ped} and was saved during the experiments, the data for the pilot position (X_N, Y_N), aircraft heading Ψ and yaw rate R were also stored during the experiment and used as input for the parameter estimation.

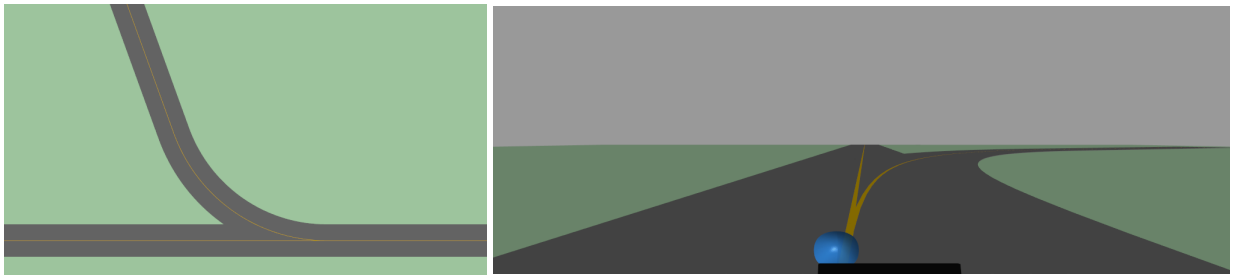

(a) Top view of the 3D environment

(b) Pilot view during the experiment

Figure 6: The Simscape Multibody environment developed for the experiment.

4.2 Parameter identification

The mechanical steering system and aircraft model were implemented in Simulink for the evaluation of the closed-loop simulation with the proposed pilot model. For the pilot-in-the-loop experiments, the same plant was used, and the proposed pilot model was also implemented in Simulink, which was used for the grey-box identification. The Parameter Estimator app was used for this identification, the setup was made using the sum of square error as the cost function, the nonlinear least square as the optimization method, and the trust-region-reflective algorithm. All the 13 model parameters that were optimized to better fit each one of the two different datasets used are shown in Tab. 1.

Table 1: Identified values of model parameters for two different pilot-in-the-loop experiments.

Parameter	**Dimension**	**Initial Value**	**Experiment 1**	**Experiment 2**	**% of variation**
$T_{LAD_{FB}}$	s	2	1.726	1.931	+11.9
K_{FB}	–	0.5	0.5893	0.6849	+16.2
T_I	s	0.05	0.0488	0.0400	-18.0
T_L	s	0.2	0.1893	0.0872	-53.9
$T_{LAD_{FF}}$	s	1	0.808	0.4128	-48.9
K_{FF}	rad.s	0.5	0.4125	0.5224	+26.6
T_{FF}	s	0.5	0.1141	0.5739	+403
K_R	s	1	0.2021	0.5086	+152
t_d	s	0.2	0.4913	0.3613	-26.5
ω_{NM}	rad/s	10	3.3542	3.7550	+11.9
ξ_{NM}	–	0.707	0.5685	0.9177	+61.4
K_n	–	0.1	0.2861	0.0983	-65.5
T_n	s	0.1	0.5037	0.9850	+95.6

The experiments considered two different levels of experience with the system dynamics. The first one was performed by the pilot after few training rounds and the second one after another set of tries. Figure 7 shows the command performed by the pilot and compares it to the command performed by its respective identified model for each of the experiments, this comparison is presented for the open-loop simulation, which means that the pilot model was simulated using the experiment data as input and comparing its output. The first pilot performance shows an oscillatory behavior which is

understandable due to the lack of experience with the system, the model was able to represent the behavior of the pilot with a similar low-frequency oscillation. Figure 7b presents the second experiment where the pilot was familiarized with the controlled dynamics, in this case, the model was also capable of representing the operator behavior, with low amplitude oscillation and smoother pattern. The Variance Account for (VAF) was used in order to validate the capability of the model output u_{sim} to predict the output signal u, the results were 98.4% and 99.2% for the first and second experiment, respectively. Table 1 shows the identified model parameters for the two experiments. Some parameters presented a large variation from the first experiment to the second one, they are the visual error lead time; the feedforward anticipation, gain and lag time; the yaw rate gain; the time-delay; the neuromuscular damping; the remnant filter gain and time.

$$VAF = \left(1 - \frac{\sum |u - u_{sim}|^2}{\sum u^2}\right) \times 100\% \tag{10}$$

Analyzing the visual error feedback contribution it can be perceived a small increase in the gain and the anticipation, additionally, a large reduction in the lead time constant, this can occurs because the look-ahead anticipation time was increased but also because when more familiarized with the plant the operator is capable of reducing its effort on previewing the error behavior. Simultaneously, experiment 2 showed that the operator increased significantly the feedforward gain and the feedforward lag time, while decreased the anticipation time of the feedforward, which indicates a smother contribution of this control path associated with a more precise starting time. The yaw rate gain increment is associated with the greater stability of the second performance damping the yaw oscillatory behavior of the pilot-aircraft system. The time delay was also reduced, but with a lower variation, it can be justified by an increase in the pilot's attention and perception of the displayed motion during the second experiment. The neuromuscular damping factor was also increased showing the damping characteristics of the second experiment performance. Finally, the contribution of the remnant is significantly reduced by the filter gain, which indicates a reduced influence of nonlinear behavior and an increase in the error perception precision.

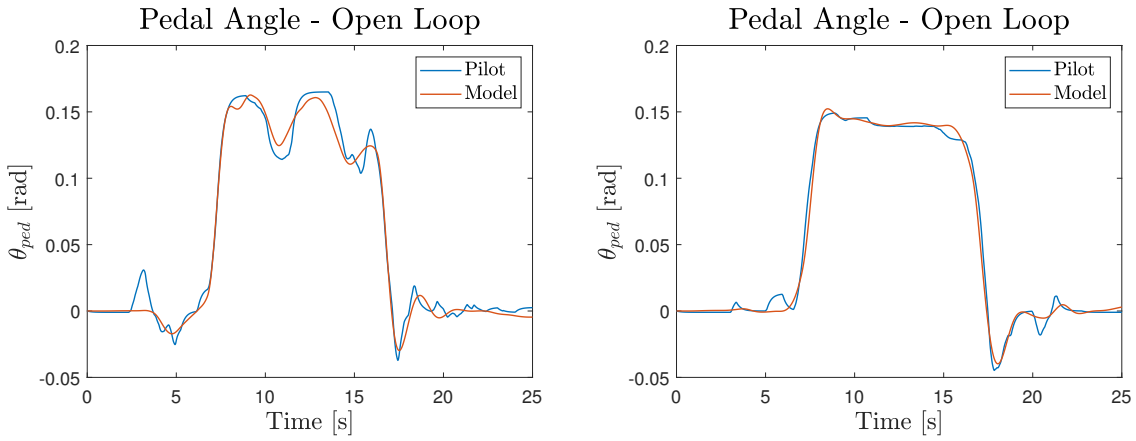

(a) First experiment, VAF = 98.4%

(b) Second experiment, VAF = 99.2%

Figure 7: Comparison between the experimental data and the identified model output in open-loop simulation for two different experiments.

The previous results consider the simulation of the pilot model in open-loop conditions, receiving the inputs from the stored experimental data. A closed-loop simulation was realized for each identified model in order to evaluate the performance when controlling the aircraft on the ground and using its feedback. The commented differences between identified behaviors for experiments 1 and 2, can be noted by the comparison of the individual control contribution of the visual feedback of heading error, the feedforward and yaw rate feedback, Fig. 8 and Fig. 9. Experiment 1 pilot individual pilot contributions presented an oscillatory behavior in each contribution due to the neuromuscular damping and the reduced gain of the yaw rate feedback control allowed the oscillations presented by the visual feedback control. In experiment 2 occurs the reverse, the yaw rate gain contributed to damp the visual feedback oscillations, besides, the feedback command is closer to a trapezoidal signal which is the expected overall result for the optimized input for the analyzed maneuver. Despite the variation between pilot and model, the trajectory comparison shows a good fit for each comparison, as a result of steering angle input differences, the yaw rate comparison presents similar variations.

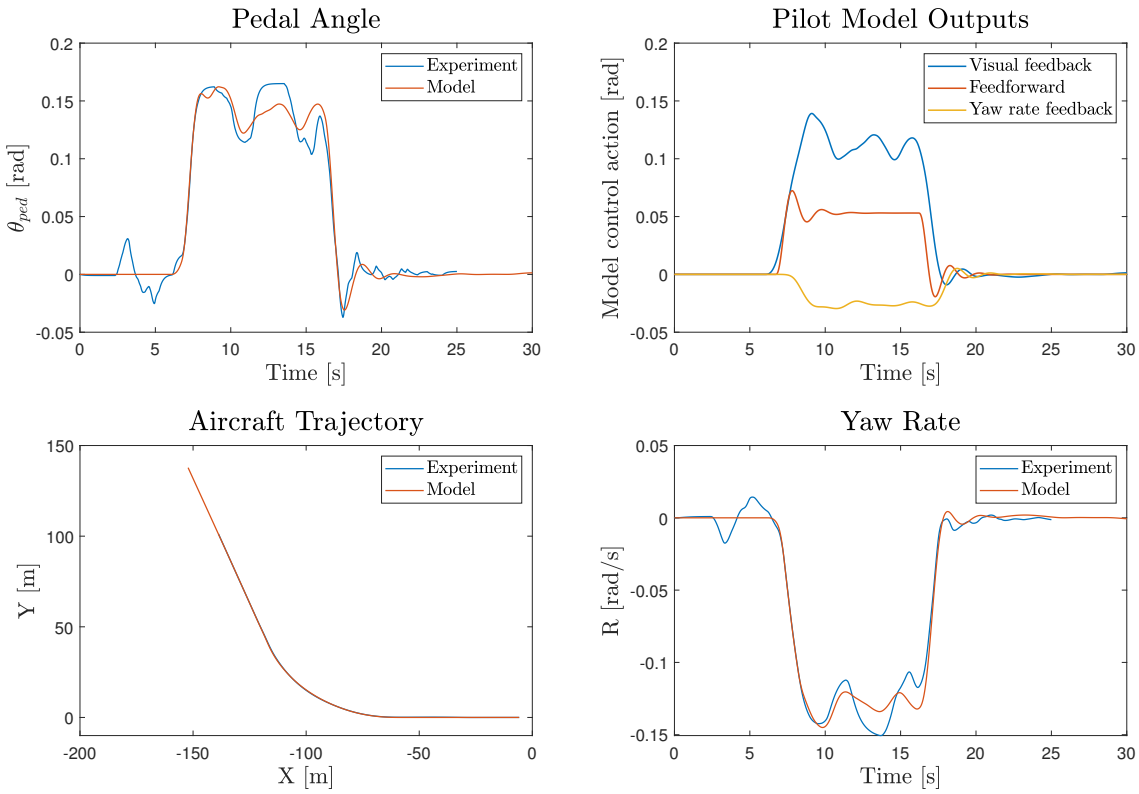

Figure 8: Closed-loop simulation of the pilot model with the parameters identified for experiment 1.

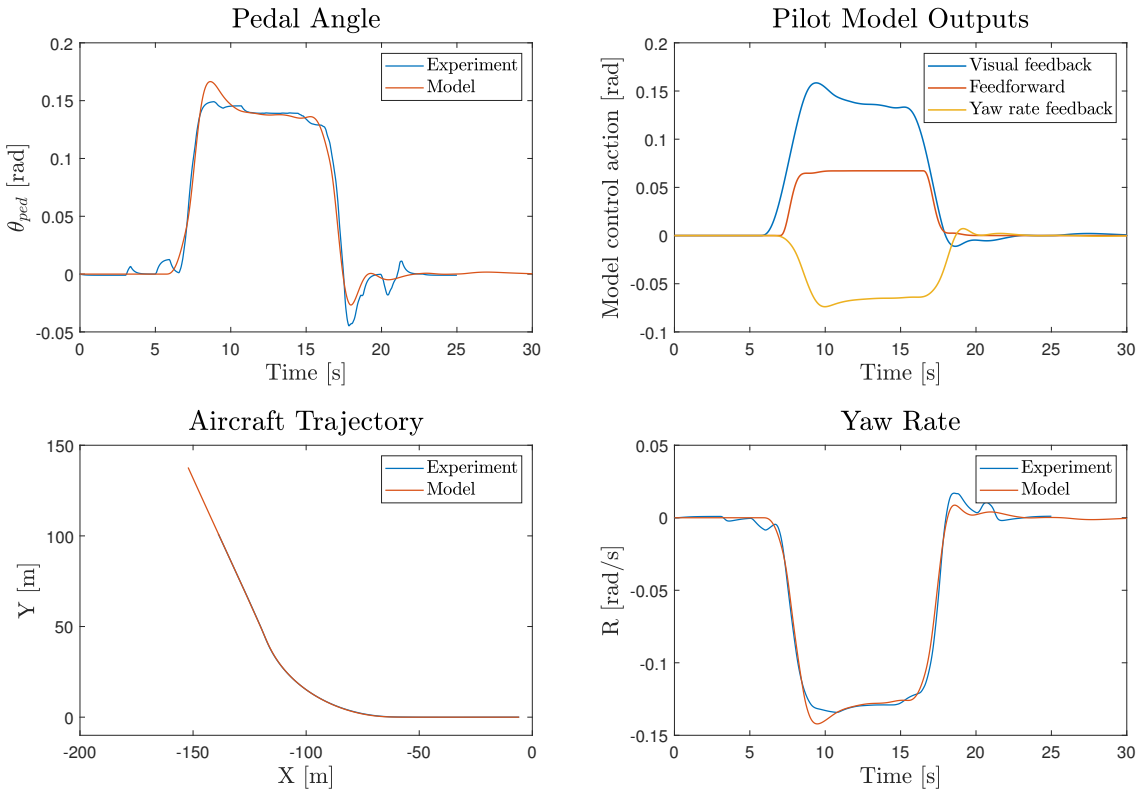

Figure 9: Closed-loop simulation of the pilot model with the parameters identified for experiment 2.

5. CONCLUSIONS

A pilot model for the nose wheel steering control of an aircraft was presented which was capable to represent two different behaviors for the same constant radius maneuver. The model uses a lead compensator for the main control component with a visual look-ahead error as input, the feedforward control was added to improve the tracking task performance, a control loop using the yaw rate was also utilized improving the model stability, the information processing delay and neuromuscular dynamics were implemented, and, finally, a modulated remnant was proposed before the linear compensator for the look-ahead heading error. The pilot-in-the-loop experiments successfully generated two different datasets for the parameter estimation that was performed by the Matlab Parameter Estimator app, using the stored experiment data as the input and optimizing the model to better fit the pilot performance. The analysis of the identification results permitted the understanding of the main characteristics that should be considered in the model to represent different behaviors.

6. REFERENCES

Amer, N.H., Zamzuri, H., Hudha, K. and Kadir, Z.A., 2017. "Modelling and control strategies in path tracking control for autonomous ground vehicles". *Journal of Intelligent and Robotic Systems*, Vol. 86, No. 1, pp. 225–254.

Drop, F., 2016. *Control-Theoretic Models of Feedforward in Manual Control*. Ph.d. thesis, Graduate Program in Aerospace Engineering, Delft University of Technology, Delft, Netherlands.

Hess, R.A., 2005. "Rudder control strategies and force/feel system designs in transport aircraft". *Journal of Guidance, Control, and Dynamics*, Vol. 28, No. 6, pp. 1251–1262.

Lone, M. and Cooke, A., 2014. "Review of pilot models used in aircraft flight dynamics". *Aerospace Science and Technology*, Vol. 34, No. 1, pp. 55–74.

Macadam, C.C., 2003. "Understanding and modeling the human driver". *Vehicle System Dynamics: International Journal of Vehicle Mechanics and Mobility*, Vol. 40, No. 1-3, pp. 101–134.

McRuer, D. and Graham, D., 1963. "Pilot-vehicle control system analysis". In *Proceedings of the AIAA Guidance and Control Conference*. AIAA, Cambridge, MA, USA.

Nash, C.J. and Cole, D.J., 2018. "Modelling the influence of sensory dynamics on linear and nonlinear driver steering control". *Vehicle System Dynamics*, Vol. 56, No. 5, pp. 689–718.

Nieuwenhuizen, F.M., Zaal, P.M.T., Mulder, M., Paassen, M.M.V. and Mulder, J.A., 2008. "Modeling human multichannel perception and control using linear time-invariant models". *Journal of Guidance, Control, and Dynamics*, Vol. 31, No. 4, pp. 999–1013.

Rasmussen, J., 1983. "Skills, rules, and knowledge; signals, signs, and symbols, and other distinctions in human performance models". *IEEE Transactions on Systems, Man, and Cybernetics*, Vol. SMC-13, No. 3, pp. 257–266.

van der El, K., Pool, D. and Mulder, M., 2014. "Measuring and modeling driver steering behavior". *Transportation Research Part F Traffic Psychology and Behaviour*, Vol. 61, pp. 337–346.

van der El, K., Pool, D. and Mulder, M., 2019. "Analysis of human remnant in pursuit and preview tracking tasks". *IFAC-PapersOnLine*, Vol. 52, pp. 154–150.

Xu, S., Tan, W., Efremov, A.V., Sun, L. and Qu, X., 2017. "Review of control models for human pilot behavior". *Annual Reviews in Control*, Vol. 44, pp. 274–291.

Zaal, P.M.T., Pool, D.M., Mulder, M. and van Paassen, M.M., 2009. "Multimodal pilot control behavior in combined target-following disturbance-rejection tasks". *Journal of Guidance, Control, and Dynamics*, Vol. 32, No. 5, pp. 1418–1428.

Zaychik, K., Cardullo, F. and George, G., 2012. "A conspectus on operator modeling". In *Proceedings of the AIAA Modeling and Simulation Technologies Conference and Exhibit*. AIAA, Reston, VA, USA.

Zhou, J. and Peng, H., 2009. "Feedforward and feedback control of lane keeping by the human driver". In *Proceedings of the ASME 2007 International Mechanical Engineering Congress and Exposition. Volume 16: Transportation Systems*. Seattle, Washington, USA.

7. RESPONSIBILITY NOTICE

The authors are solely responsible for the printed material included in this paper.